



A temporal and spatial analysis of anthropogenic noise sources affecting SNMR



E. Dalgaard ^{a,*}, P. Christiansen ^b, J.J. Larsen ^c, E. Auken ^a

^a HydroGeophysics Group, Department of Geoscience, Aarhus University, Denmark

^b Department of Physics, Aarhus University, Denmark

^c Department of Engineering, Aarhus University, Denmark

ARTICLE INFO

Article history:

Received 11 April 2014

Accepted 21 August 2014

Available online 28 August 2014

Keywords:

SNMR

Electromagnetic noise

Signal processing

Hardware development

ABSTRACT

One of the biggest challenges when using the surface nuclear magnetic resonance (SNMR) method in urban areas is a relatively low signal level compared to a high level of background noise. To understand the temporal and spatial behavior of anthropogenic noise sources like powerlines and electric fences, we have developed a multichannel instrument, noiseCollector (nC), which measures the full noise spectrum up to 10 kHz. Combined with advanced signal processing we can interpret the noise as seen by a SNMR instrument and also obtain insight into the more fundamental behavior of the noise. To obtain a specified acceptable noise level for a SNMR sounding the stack size can be determined by quantifying the different noise sources. Two common noise sources, electromagnetic fields stemming from powerlines and fences are analyzed and show a $1/r^2$ dependency in agreement with theoretical relations. A typical noise map, obtained with the nC instrument prior to a SNMR field campaign, clearly shows the location of noise sources, and thus we can efficiently determine the optimal location for the SNMR sounding from a noise perspective.

© 2014 Elsevier B.V. All rights reserved.

1. Introduction

The surface nuclear magnetic resonance (SNMR) technique dates back to the late 1970's with the Russian invention, the Hydroscope, which succeeded in detecting signals from water in the subsurface. Since then developments in the instrumentation (Bernard, 2007; Walsh, 2008), signal processing (Dlugosch et al., 2011) and inversion algorithms (Behroozmand et al., 2012; Müller-Petke and Yaramanci, 2010) have pushed the method to become a generally applicable tool for groundwater characterization (Knight et al., 2012; Ryom Nielsen et al., 2011).

One of the biggest challenges of the method when using it in urban areas is the relatively low signal level compared to the high level of background noise. The first generation of SNMR instruments were single channel instruments. With single channel instruments, both magnetic resonance excitation and signal recording are performed with one single loop. Typical signal filtering are stacking, notch filtering (Legchenko and Valla, 2003) and Fig. 8 loop geometry (Trushkin et al., 1994). These techniques suppress in particular noise from powerline harmonics (Legchenko and Valla, 2003). Unfortunately these techniques have significant drawbacks; notch filters may distort the SNMR signal and Fig. 8 loop has a complicated sensitivity function and the

depth of penetration is decreased. With the introduction of the multichannel SNMR system more sophisticated noise reduction techniques became possible (Walsh, 2008). With the multichannel technique it is possible to avoid the drawbacks from the single-channel SNMR filtering techniques (Jiang et al., 2011), which have improved the efficiency of the method. Recently an approach where filtering the noise from the powerline harmonics by modeling the harmonics has been suggested (Larsen et al., 2013). The method can be combined with multichannel filtering (Dalgaard et al., 2012; Müller-Petke and Costabel, 2013), which has pushed the signal processing to obtain even higher signal to noise ratios (S/N).

Signal processing is an integral part of getting SNMR soundings with an acceptable S/N. However, the influence of noise is still the most important parameter affecting the measurement time. Methods to locate the sources are therefore needed to determine the optimum placement of the SNMR measurements and thereby obtain higher S/N ratios and shorter measurement times. To locate noise sources and investigate the spatial and temporal variations of the noise, we have developed an instrument, noiseCollector (nC). The nC is a two channel system and built to resemble a SNMR instrument so that noise sources are measured and analyzed in a way similar to "real" SNMR data.

In this paper we will discuss the details of the system and the signal processing. Temporal and spatial analysis of noise sources with the nC instrument are shown, and results for different typical noise sources are presented. Then results from a thorough spatial noise mapping prior to a SNMR field campaign are shown, and we introduce a combined

* Corresponding author at: C. F. Møllers Alle 4, 8000 Aarhus C, Denmark. Tel.: +45 40419842.

E-mail address: ebd@qeye-labs.com (E. Dalgaard).

point measurement method to reduce field time spent on comprehensive noise maps. This method is used to locate noise sources based on only 3 point measurements, and by that an optimized location of SNMR measurements can be determined. Finally it is shown how nC data correlates with SNMR data. This correlation is needed to predict how noise sources affect the SNMR sounding and to estimate the stacksize necessary to obtain an acceptable signal to noise ratio.

2. Method and methodology

2.1. noiseCollector design

The nC instrument is designed to resemble a SNMR system in terms of sampling rate and bandwidth. The core of the nC is a 2 channel, 16 bit PICOscope 4262 analog to digital converter (ADC) able to sample up to 5 MHz (Fig. 1). The electromagnetic noise is measured in up to two receiver induction coils with a bandwidth of more than 100 kHz. Attached directly to the coils is a frontend amplifier with a gain factor of 21. In the nC box the signal is further amplified with a gain factor of 24, then low pass filtered by a fourth order analog low pass filter with a cutoff frequency at 6 kHz before entering the ADC. The data acquisition is controlled from a laptop connected directly to the nC box. The adjustable settings of the ADC are sampling frequency, measurement duration and voltage range. All data presented in this paper have been obtained using 10 by 10 m² loops with 7 turns, a sampling frequency of 20 kHz, a measurement duration of between a few seconds and a few minutes, and the voltage range chosen so we obtain the highest possible signal resolution without saturating the ADC. A built in computer was not included in the design of the instrument as it was important to minimize the internal electronic noise.

2.2. nC data examples

In Fig. 2 two typical measurements obtained by the nC are shown. Data were collected in the Kasted area, Denmark (Fig. 2A). Fig. 2B shows a time domain plot of data collected at a site highly dominated

by harmonics from a nearby power cable seen as a repeating pattern. Transferring the data to the frequency domain (Fig. 2C) harmonics with a base frequency of 50 Hz are clearly seen. Around 4 kHz the signal amplitude decreases due to the low pass filter of the nC. The inset in Fig. 2C shows a zoom at the relevant frequencies for SNMR, which in this part of the world are close to 2 kHz. It is seen that the base power level is around -70 dB and the harmonics are between -40 and -50 dB. Fig. 2D shows a time domain plot of data collected at a site dominated by spikes. The spikes are produced by electrical discharges in a nearby electric fence. Note the scale difference of a factor of 30 between Fig. 2B and D. Fig. 2E shows the data transferred to the frequency domain. It is clear that the spike has a minor content of low frequencies and also that harmonics are present, but to a much lesser degree compared to the other site in Fig. 2B. A base level around -50 dB is seen, which is 20 dB higher than the other site. The different base level is due to the distortion from the spike. Based on the plots in Fig. 2, two distinct electromagnetic features are observed, namely powerline harmonics and spikes coming from electrical discharges. A quantification of these is necessary in order to predict the quality of the data at a site.

2.3. Processing

Raw data obtained by the nC, $w(k)$, consists of spikes, $s(k)$, correlated noise, $c(k)$ and random noise, $r(k)$.

$$w(k) = s(k) + c(k) + r(k) \quad (2.1)$$

The majority of correlated noise in urbanized areas comes from the 50/60 Hz harmonics from powerlines and power cables. Signal processing is done in two steps, de-spiking followed by a harmonic filtering.

The de-spiking procedure (Dalgaard et al., 2012) is semi-automatic and a spike is detected in the time domain when the voltage induced in the loop gets higher than a defined threshold. In some cases low amplitude spikes can be hard to detect. Thus, to emphasize the spikes,

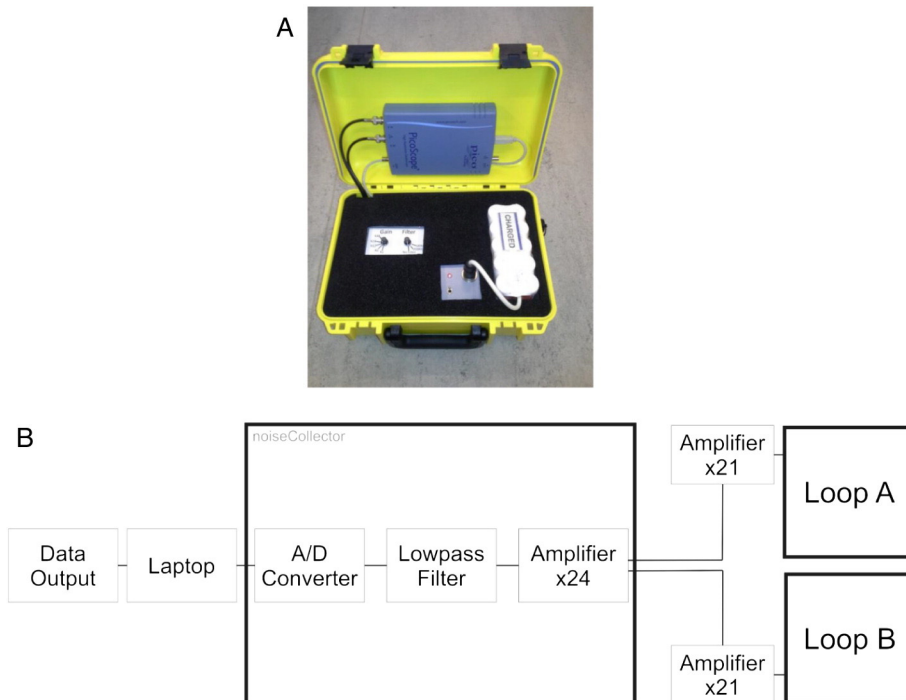


Fig. 1. A) Picture of the nC instrument. B) Block diagram of the nC. The system is a two channel system. The signals are obtained in loops A and B, subsequently an amplification in the frontend amplifier of 21 is applied. The recorded signals then enter the nC box and are amplified with a gain of 24. The amplified signals are lowpass filtered at 6 kHz and after this the A/D conversion is performed. The laptop controls and receives data from the system.

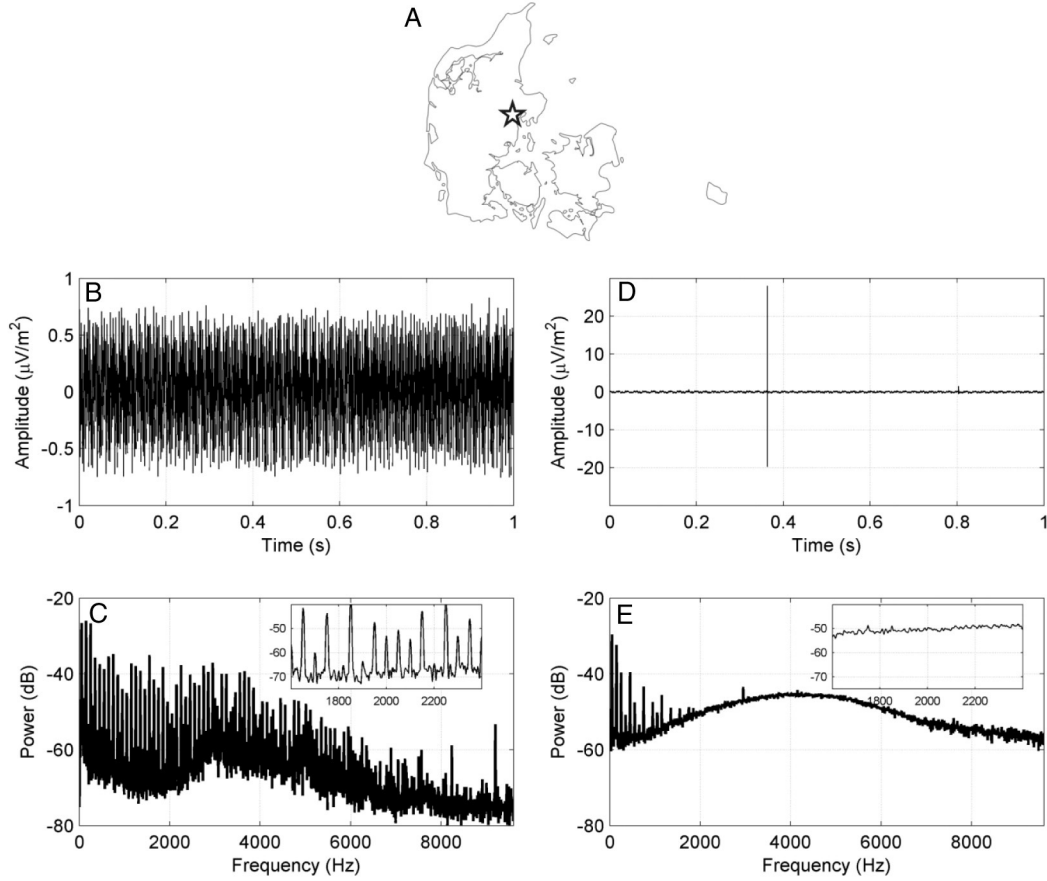


Fig. 2. Example datasets from two measurements obtained by the nC at the Kasted area, Denmark (A). The left contains powerline interference (B and C) and the right contains a spike from a fence (D and E). The top figures show the measurements in the time domain. The lower figures show the same measurements in the frequency domain, the inset shows a zoom of the frequencies around 2000 Hz. In the y-scale 0 dB correspond to 1 $\mu\text{V}/\text{m}^2$.

the signal is transformed into a nonlinear energy operator domain (Mukhopadhyay and Ray, 1998).

The spike threshold is determined by a median absolute deviation. For a time series, $\bar{x} = \{x(k) \dots x(k+N-1)\}$, it is defined as (Hoaglin et al., 2000):

$$\text{MAD} = \text{median} \{ |\bar{x} - \text{median} \{ \bar{x} \} | \} \quad (2.3)$$

Where the median of the time series, \bar{x} , is subtracted from the time series, the absolute values are calculated and the median of this defines the median absolute deviation value. This median absolute deviation value is multiplied by a user defined factor, typically in the order of 10–20 (Dalgaard et al., 2012), and defines the threshold. Samples containing spikes are ignored during the subsequent harmonic filtering, and thus the samples identified as spikes are not included in further calculations.

The implementation of the harmonic filtering follows the procedure described by Larsen et al. (2013). The harmonics $h(k)$ are modeled as:

$$h(k) = \sum_{m=1}^{200} A_m \cos\left(2\pi m \frac{f_0}{f_s} k + \varphi_m\right) \quad (2.4)$$

where f_0 is the fundamental frequency, f_s denotes the sampling frequency and A_m and φ_m are the amplitude and phase of the m 'th harmonic component. The summation over m extends over all harmonics within the Nyquist criterion, thus all harmonics until 10 kHz, which correspond to m in an interval from 1 to 200. The unknown parameters to be determined in this model are f_0 , A_m and φ_m , each of these parameters is a function of time. It is our experience that by dividing the time series

into segments of 1 second, the parameters are approximately constant and an independent harmonic filtering of the segments can be carried out. The fitting of A_m and φ_m is a linear optimization problem, whereas the fitting of f_0 is a nonlinear problem. The modeling of the harmonics is performed in two steps. The first step is the determination of f_0 and the second step is a linear fitting of A_m and φ_m . The value of f_0 for the powerlines in Denmark is known to be in a narrow band around 50 Hz; other harmonic sources and powerlines in other countries can have another base frequency. To locate the precise position of f_0 , a search of the peak value of the correlation between the recorded data and a pure sinusoid with frequencies varying with sequential steps around 50 Hz is performed. The search is performed iteratively with an increasing resolution of the test frequencies of the pure sinusoid. The resulting precision of the determination of f_0 is approximately 1 mHz.

For the fitting of the linear parameters the cosine term in Eq. (2.4) is rewritten as:

$$A_m \cos\left(2\pi m \frac{f_0}{f_s} k + \varphi_m\right) = \alpha_m \cos\left(2\pi m \frac{f_0}{f_s} k\right) + \beta_m \sin\left(2\pi m \frac{f_0}{f_s} k\right) \quad (2.5)$$

where the variables are related as:

$$A_m = \sqrt{\alpha_m^2 + \beta_m^2} \text{ and } \varphi_m = \tan^{-1}\left(\frac{\beta_m}{\alpha_m}\right). \quad (2.6)$$

α_m and β_m are fitted for all m with a least squares approach.

In the case of an ideal de-spiking and an ideal filtering of correlated noise the signal is only corrupted by random noise. In SNMR random

noise is suppressed by stacking a number of independent measurements (N_S). Assuming Gaussian distributed noise, the data standard deviation will decrease as:

$$\text{STD}_{\text{stacked}} = \frac{1}{\sqrt{N_S}} * \text{STD}_{\text{ini}}. \quad (2.7)$$

Here the initial standard deviation on data is given by STD_{ini} , and the resulting reduced standard deviation by $\text{STD}_{\text{stacked}}$. By knowing STD_{ini} it is possible to estimate the number of measurements needed to obtain an acceptable $\text{STD}_{\text{stacked}}$.

The root mean square (RMS) is used to compare the energy of the noise signals and is defined as:

$$\text{RMS} = \sqrt{\frac{1}{n} (x(1)^2 + x(2)^2 + \dots + x(n)^2)}. \quad (2.8)$$

Here x is the voltage of the signal. This RMS value is referred to as the noise level of a location with a certain timestamp

$$\text{RMS}(T_0, P_0) \quad (2.9)$$

where P_0 is a location of the receiver, and T_0 is the timestamp.

3. Reference technique

The reference technique is a way to compensate for the temporal variation of electromagnetic sources. The source amplitude ratio (SAR), which is the ratio between RMS values at two different measurement times, T_k and T_0 , at the same point, P_{ref} , is defined as:

$$\text{SAR}(T_k) = \frac{\text{RMS}(T_k, P_{\text{ref}})}{\text{RMS}(T_0, P_{\text{ref}})} \quad (3.1)$$

The technique assumes that all points will follow the same temporal evolution i.e. the spatial noise pattern is unchanged. Considering a single source, this source can be accounted for with:

$$\text{RMS}(T_k, P_j) = A_S(T_k) \cdot f(r_j) \quad (3.2)$$

where $A_S(T_k)$ represents the amplitude of the generated noise source at timestamp T_k , $f(r_j)$ is a function that describes a spatial dependency of a source, which depends on the distance between the source and the receiver, r_j , i.e. for an infinitely long cable $f(r_j) = \frac{1}{r_j}$.

The ratio between a reference point and adjacent points is formed by:

$$\frac{\text{RMS}(T_k, P_{\text{ref}})}{\text{RMS}(T_k, P_j)} = \frac{A_S(T_k) \cdot f(r_{\text{ref}})}{A_S(T_k) \cdot f(r_j)} = \frac{f(r_{\text{ref}})}{f(r)} = \text{constant}. \quad (3.3)$$

If the single source assumption is correct then equation 3.3 demonstrates that all points follow the same pattern. If the noise in the reference point increases with a certain factor, then the point P_j increases with the same factor. This factor is applied on all points adjacent to each other down to a common reference time.

4. Temporal variation

Electromagnetic signals are not constant over time, for example power cables to households emit noise of varying strength depending on the load from the different electrical components in the house. The signal level at a given location is fluctuating over time and therefore $\text{RMS}(T_0, P_0) \neq \text{RMS}(T_1, P_0)$. The temporal variation of noise complicates the analysis because a comparison between locations will be different due to the temporal changes. This means that best practice would be to measure several locations at the same time. The nC has two channels; thus two simultaneous measurements are possible, $\text{RMS}(T_0, P_0)$ and

$\text{RMS}(T_0, P_1)$. When several simultaneous measurements are needed on several locations, the temporal variation can be overcome by using the reference technique described in previous section. The reference technique uses the SAR-value to estimate the noise level of several points back to the T_0 timestamp.

$$\text{RMS}(T_0, P_{\text{ref}}) = \text{RMS}(T_k, P_{\text{ref}}) \text{SAR}(T_k) \quad (4.1)$$

4.1. Results

In this section the validity of the SAR value and hence the reference technique is investigated. In order to examine the limitations of the technique the SAR-value is tested under circumstances that violate the single source assumption. The technique is applied in an area with several strong noise sources located in different directions; an electric fence is located 150 m to northwest, a high voltage powerline is 1.2 km to the north, some buildings 150 m to the southeast, and an underground power cable 250 m to the south. The receiver loops stay at the same position separated by 50 m and the measurements are carried out over a 10 hour period. The RMS-values were measured every 15 minutes from 20 second time series; these are denoted $\text{RMS}(T, P_0)$ and $\text{RMS}(T, P_1)$. Fig. 3A shows the RMS without any processing, Fig. 3B shows the RMS of the modeled harmonic content and Fig. 3C shows the remaining RMS after processing. The three plots are divided into two subplots where the upper plot displays the RMS-value of two points at different timestamps and the lower displays a ratio given by

$$\text{Ratio}(T_i) = \frac{\text{RMS}(T_i, P_1)}{\text{RMS}(T_i, P_2)} \quad (4.2)$$

The ratio is found to be time dependent, where within the SAR approximation they should actually be constant.

$$\frac{\text{RMS}(T_i, P_1)}{\text{RMS}(T_i, P_2)} = \frac{\text{SAR}(T_i) \text{RMS}(T_0, P_1)}{\text{SAR}(T_i) \text{RMS}(T_0, P_2)} = \frac{\text{RMS}(T_0, P_1)}{\text{RMS}(T_0, P_2)} = \text{Ratio}(T_0) = \text{constant} \quad (4.3)$$

The observed time variation of the ratio in (Eq. (4.3)) is a way to evaluate the applicability of the reference technique.

The experiment shows that there is a temporal variation in the noise field. An extreme example is a drop from more than 400 nV/m² to less than 100 nV/m² in the RMS of the raw data during 1 hour from 19:30 to 20:30. If a spatial dependency experiment were to be performed during this hour, it would be useless without the reference technique. In Fig. 3A two events are seen at 10.45 and 19.30 with high RMS values, these high RMS values for the raw data are due to the power cable harmonics, as seen in Fig. 3B where similar events are observed. The trends and the amplitudes of the RMS values in Fig. 3B follow the trends and the amplitudes in Fig. 3A, as the measured signal is highly dominated by power cable harmonics. Fig. 3C shows the processed data and it is seen that the RMS level is around 15 nV/m² and the variation with time is much less than the raw data (note that the RMS scale has been changed by a factor of 10). On average the RMS is decreased by a factor of 10 after processing.

In the RMS plots in Fig. 3 the values from position 0 and 1 follow each other quite closely. As expected the ratio is not constant because the single source assumption is wrong. The standard deviation of the ratio gives an estimate of the degree to which the single source assumption is violated. The mean of this ratio over the experiment is plotted together with the actual ratio at each given time. The raw data in Fig. 3A gives a ratio of 0.639 ∓ 0.081 . The harmonics content gives a ratio of 0.639 ∓ 0.102 and the processed data in Fig. 3C has a ratio of 0.581 ∓ 0.069 . From similar experiments at other sites in Denmark, results with ratios and standard deviations in the same order of magnitude are obtained. Based on these temporal variation

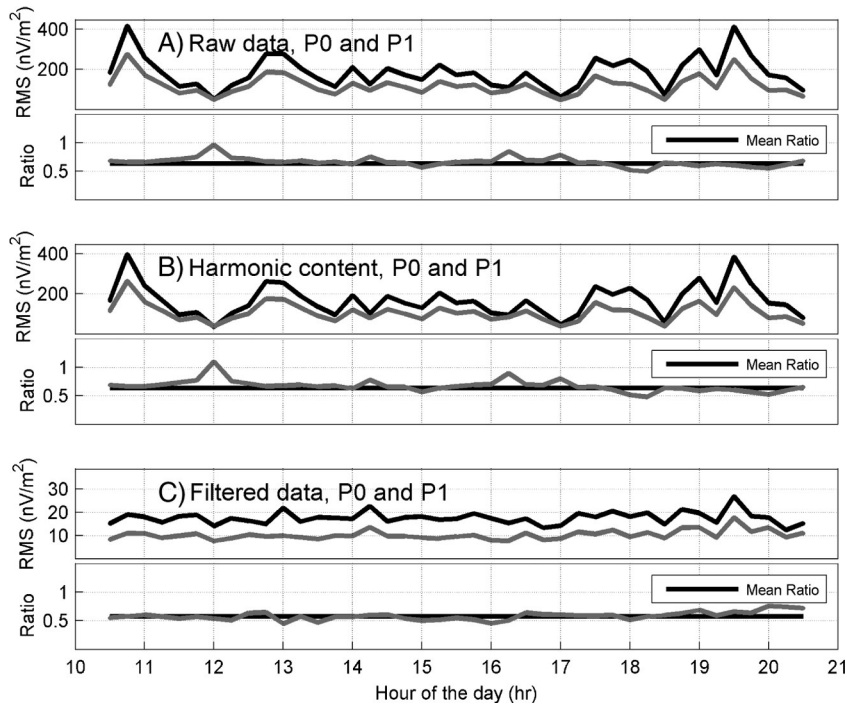


Fig. 3. A 10 hour experiment with 20 seconds measurements obtained every 15 minutes at two positions, 0 and 1 (black and grey) separated with a distance of 50 m. The upper subplots in each section are: A) RMS values of the raw signal, B) RMS values of the modeled harmonic content and C) RMS values of the remaining signal after noise processing. The lower subplots contain the ratio between the RMS values from the two positions at each measurement (grey) and an average value for the entire experiment (black).

experiments an error in the noise estimate on the order of 10% is expected with the reference technique. Without the reference technique the temporal noise variation would propagate introducing much larger errors in the noise estimate, at this site up to 400%.

5. Spatial variation

In this section the spatial dependency of noise sources will be investigated. Some assumptions about the electromagnetic noise sources are needed to express them mathematically. First it is assumed that all fences and cables encountered are infinitely long. This is obviously not true, but it simplifies matters. Second it is assumed that sources from harmonic content with the same base frequency originate from a single source. Different harmonic sources with the same base frequency cannot be distinguished, as those sources will add together and appear as one. Magnetic dipoles are a potential source of noise but are not considered in this study.

5.1. Noise from an infinitely long cable

An infinitely long cable with a current will generate an electromagnetic field, which falls off as $1/r$ from the wire, where r is the distance between the receiver and the source. High voltage power cables most often consist of three twisted wires with a voltage phase offset of 120 degrees. A historical overview in mitigation of electromagnetic fields using three-phase four-wire twisted cables is given by Yang et al. (2013). Away from the source the field from three phases cancels and the distance dependency changes from $1/r$ to $1/r^2$. The resulting alternating electromagnetic field, B , is proportional as:

$$B \propto \frac{\sin(\omega_S t)}{r^2}. \quad (5.1)$$

The main component of the electromagnetic field alternates with an angular frequency equal to the frequency of the source, $\omega_S \cong 2\pi \cdot 50$ Hz; other components of the electromagnetic field are present as harmonics. The electromagnetic field induces an alternating voltage in

the receiver loop. The signal level in a measurement is defined by the RMS of the signal measured at time T_0 and location P_k :

$$\text{RMS}(T_0, P_k) = \frac{A_S(T_0)}{r^2} \quad (5.2)$$

where $A_S(T_0)$ is the time-varying source amplitude that depends on the specific source.

5.2. Noise from an infinitely long fence

Spikes in signals are a result of electrical discharges, typically from electrical fences or lightning. A spike is characterized in the time domain as being short and with a high induced voltage. The amplitude of the spike drops when moving away from a source. Infinite fences with one wire generate spikes that fall off as $1/r$. Fences encountered in the field that have more than one wire will have a different distance dependency. A fence generates the electrical impulses with a constant repetition rate and amplitude; hence it is possible to separate different spike sources based on these characteristics.

5.3. Measurements of a harmonic source

Measurements were performed at several sites which all show that Eq. (5.1) adequately describes the spatial dependency of a harmonic source. In Fig. 4 a plot of 38 point measurements recorded 50 to 450 m from a harmonic source from a high voltage powerline. The powerline continues in a straight line for at least 2.5 km at both ends. For this experiment the reference technique was used. The inset shows the location of the powerline relative to the point measurements. These are plotted from GPS coordinates, which are also used to calculate the distance from the wire to each of the points. The figure displays the RMS value as a function of distance to the power line. Three points are indicated with a grey color. These outlying points are excluded when fitting to Eq. (5.2) as they are influenced by another harmonic source

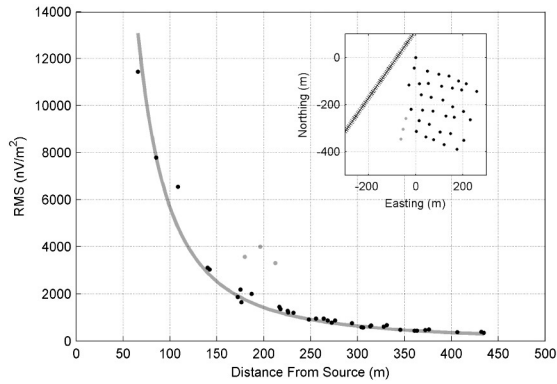


Fig. 4. Radial dependency of the electromagnetic field from a power line source. The large figure contains 38 point measurements. The RMS-value is a function of the distance between the point measurement and the powerline. The grey line is a fit of the point measurements to the expression $1/r^2$. The inset displays the relative locations of the point measurements and the powerline (grey railway line). The point measurements marked as grey are discarded in the fit.

located in the southeast corner. The fit of the remaining points indicates a good agreement with the $1/r^2$ relation.

5.4. Measurements of noise from a fence

Fig. 5 shows measurements of spike amplitudes as a function of the distance from a fence. The inset shows the fence and the measurement locations. The first thing to note is that there is both a far field and a near field relation. The three points near the fence within 75 m have a nearly constant spike amplitude. A continuous drop in the spike amplitude is observed going from 10,000 nV/m² in the near field to around 1000 nV/m² at a distance of 200 m. A $1/r^2$ relation for the far field is obtained.

The near field variations in the measurement stem from a variation of the receiver altitude relative to the fence and receiver orientation. The measurements were performed at a site with topographical variations and since the two wires in the fence are separated by 40 cm, near to the fence the measurements are sensitive to both the altitude and orientation of the receiver coils.

5.5. Noise maps

Fig. 6 shows an example where noise is measured over a 400 × 400 m field. This site is a good test site containing several different noise sources: housing to the south, an electric fence in the northwest end, a house

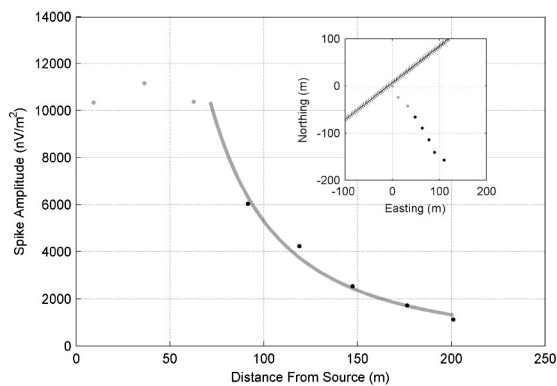


Fig. 5. Radial dependency of the electromagnetic field from a spike source. The figure displays the spike amplitude as a function of the distance between the point measurement and the fence. The grey line is a fit of the point measurements to the expression $1/r^2$. The inset displays the relative locations of the point measurements and the fence (grey railway line). The measurements marked as grey were discarded.

400 m further northeast and a high voltage powerline 1 km to the northwest. Thirty-eight points were measured; noise was measured for 30 seconds. With the current instrument it took around 9 hours to collect the data for the map, and the RMS values were calculated using 5 seconds of the noise record. Fig. 6A shows the RMS of the raw data. The highest RMS values, up to 500 nV/m², are observed at the south end of the site close to the houses. The RMS value drops faster going north compared to going in a northwest direction. The smaller drop in the RMS value in the northwestern direction is due to an electric fence located right next to the site and surrounding the field at northwest. In Fig. 6B the spike content is shown. The spike amplitude is very high next to the fence in the northwest end of the site and decreases with distance in all directions. In Fig. 6C the modeled harmonic content of the measurements is shown. It is seen that the harmonic contribution originates from houses supplied by power cables as the pattern and amplitude of the RMS from the harmonics and the raw data follow each other to a high extent. The main deviation is that the RMS value for the harmonics drops more in the northwestern direction towards the fence compared to the raw signal. The harmonic content from the high voltage powerline is not observed. In Fig. 6D the data are shown after signal processing. It should be noted that the RMS values of the remaining signal after processing are at least 10 times smaller than the raw signal. The processed signal has the highest RMS values close to the houses in the southern end of the site and the smallest values in the field in the northeastern direction. The RMS value becomes higher again going north. This is probably caused by a farm house located around 200 m further north. The remaining noise after processing is approximately white and has a clear direction towards the houses. In the northeast end the noise level after processing is below 10 nV/m²; this is still a very high level. In this example, additional information from the northeast would likely lead to a location with a lower noise level. Alternatively a Fig. 8 shape loop could be considered if moving the loop is not an option. Even though the noise is white there is a correlation between noise measured at different points implying that further noise reduction with a multichannel noise cancellation approach is possible (Dalgaard et al., 2012).

6. Combining point measurements to locate sources

From a complete noise map it is easy to locate noise sources but they are time consuming to produce. In the case with the 38 point measurements for the map the data acquisition took around 9 hours. For this reason we have developed an alternative method where fewer measurements are needed. We have called this method the combined point measurements method (CPMM). With the CPMM an adequate understanding of the noise sources can be obtained by only 3 point measurements. The main points of the CPMM are as follows:

- The CPMM method can estimate the direction of several spike sources and harmonic sources with different base frequencies. Different harmonic sources with the same base frequency cannot be distinguished, as those sources will add up and appear as one. Thus it is assumed that the harmonic content for each base frequency originates from only one single source.
- The noise sources encountered are typically not point-sources, but long cables or fences. In CPMM it is assumed that all cables and fences are infinitely long. This simplifies the calculations by limiting the number of unknown variables needed to locate a source.
- To perform a CPMM at least three simultaneous measurements are needed. The nC has two channels; thus the reference technique is used to obtain these measurements. The position of one receiver is fixed, while the other receiver is relocated for each measurement. With this technique several measurements are performed and extrapolated to the RMS values of timestamp T_0 .

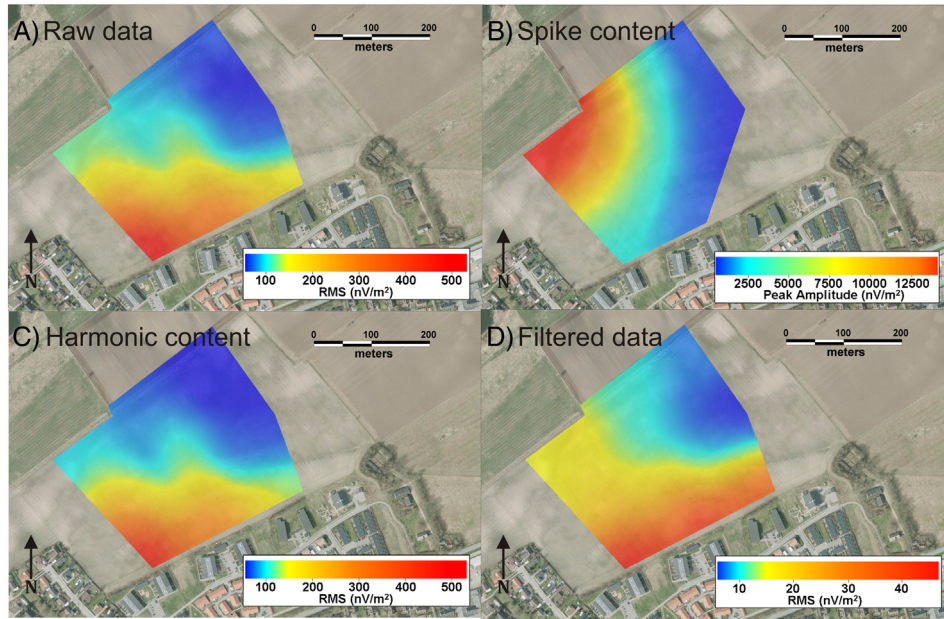


Fig. 6. A) Map illustrating the RMS value of the raw data. B) Map illustrating the spike amplitude. C) Map illustrating the RMS value of the modeled 50 Hz harmonics. D) Map illustrating the RMS value of the processed data. All maps are based on 38 point measurements and interpolated with an inverse distance weighting having a search radius of 100 m.

Long buried cables, which are usually located parallel to roads, are easy for the CPMM to locate. The applicability of CPMM is more troublesome in the vicinity of buildings, where power is distributed through many short cables. However, the short length of the cables will cause the noise to fall off faster and the currents they carry are considerably smaller.

6.1. Calculating the source location

In the CPMM the source is assumed to be an infinitely long wire. The location can be described as a line in a coordinate system.

$$y = ax + b \quad (6.1)$$

The parameters a and b determine the location of the wire. The distance from a point $P_k(x_k, y_k)$ to the line is given by

$$R(P_k) = \frac{|y_k - (a \cdot x_k + b)|}{\sqrt{1^2 + a^2}} \quad (6.2)$$

Combining (Eqs. (5.2) and (6.2)):

$$\text{RMS}(T_0, P_k) = A_S(T_0) \frac{1 + a^2}{(y_k - a \cdot x_k - b)^2} \quad (6.3)$$

The equation above has three unknown variables a , b and $A_S(T_0)$; therefore at least three measurements are needed to solve this as a non-linear least squares problem. The following cost function is minimized:

$$S(a, b, k) = \sum_{k=1}^n r_k^2 = \sum_{k=1}^n \left(A(T_0) \frac{1 + a^2}{(y_k - a \cdot x_k - b)^2} - \text{RMS}(T_0, P_k) \right)^2 \quad (6.4)$$

Here n denotes the number of point measurements.

6.2. CPMM results

Fig. 7 shows a CPMM measurement with a total of 4 point measurements. In the figure both the estimated and the actual location of a buried cable is shown. It is seen that the buried cable is not a straight line, but has two corners where the direction of the cable changes. The CPMM method assumes a straight line; thus the corners of the cable cannot be recovered. The method recovers the position of the buried cable well. With this method an estimate of where the powerlines and buried cables are located and most important where an SNMR measurement with an acceptable noise level is possible. This is discussed in the following section.

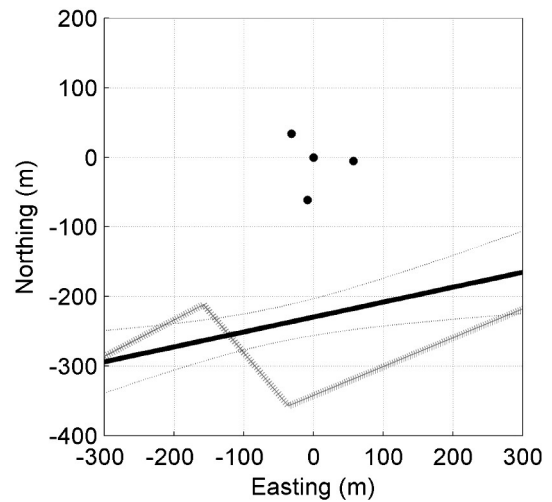


Fig. 7. A demonstration of the CPMM method. The points indicate the locations of 4 point measurements. The location of a buried cable is indicated with a grey railway line. The black line indicates the CPMM estimated location of the buried cable, together with the confidence interval of one standard deviation.

7. Correlation between SNMR and nC data

A correlation between the nC and a SNMR instrument is needed in order to use the nC data to predict how noise sources will influence a SNMR sounding. To obtain the relation between nC data and SNMR data the following measurement was performed.

An electromagnetic signal source was set up at a low noise location and the signal from this was measured (Fig. 8). The source consisted of a portable power generator, a function generator, a stereo amplifier and a coil (2.5 by 2.5 m, 7 turns). The signal used in this experiment was a sine wave at a frequency of 2100 Hz. The emitted signal was collected in loop B, around 20 m from the signal source, and measured either by the nC or the SNMR equipment. The stability of the signal source was monitored at loop A which continuously measured with the nC. The Larmor frequency of the SNMR system was set to the same frequency as the noise source. To compare the two systems as directly as possible, a digital bandpass filter similar to the bandpass filter of the NUMIS Poly is applied to the nC data: a filter centered at 2100 Hz with a bandwidth of 150 Hz. The NUMIS Poly system was self-calibrated with the signal source off; after this it measures data with the signal source set at different amplitudes.

The results of the experiment are plotted in Fig. 9. The RMS values of the SNMR measurements are plotted against the RMS values of the nC measurements. Together with the data points a reference line, which indicates the 1:1 correlation, is plotted. It is seen that the data points are in good agreement with the desired 1:1 correlation.

Based on the results it is now possible to perform nC measurements and predict how the noise conditions will influence a SNMR sounding. In the methodology section it was shown how spikes and different harmonic sources can be modeled and identified. By identifying those noise sources and subtracting them from the raw signal an estimate of the remaining noise is obtained, and from this the stacksize needed to reach an acceptable noise level can be determined. Eq. (2.7) gives the relation of stacksize and achieved noise level for uncorrelated data. By filtering spikes and harmonic noise sources, the remaining signal is not necessarily contaminated with only uncorrelated noise, as other spatially correlated noise sources might be present (Larsen et al., 2013). If this is the case these can be filtered with a multichannel approach, where transfer functions between the coils can be calculated by a Wiener filter (Dalgaard et al., 2012; Müller-Petke and Costabel, 2013). Thus the prediction from the nC of the SNMR affecting noise sources is a conservative prediction.

8. Conclusion

An instrument, noiseCollector, for measuring and mapping noise sources in a SNMR context has been demonstrated and tested in the field. The nC has proved itself to be an effective tool for noise characterization and mapping as it provides an easy way to separate the contributions from different noise sources. Important noise sources to separate

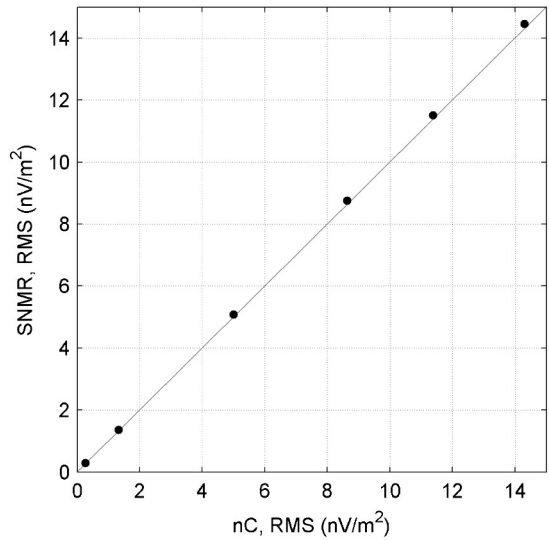


Fig. 9. RMS values for a SNMR system plotted against the RMS values for the nC system at different noise levels.

are spikes coming from electrical discharges and electromagnetic radiation from powerlines and other electrical components.

The theoretical distance relations for electromagnetic fields emitted from electrical fences and powerlines have been discussed in detail. The electromagnetic fields coming from powerlines and fences were analyzed with the nC and showed $1/r^2$ dependencies in agreement with theoretical relations. A typical noise map obtained with the nC prior to a SNMR field campaign was demonstrated and clearly showed where noise sources were located and where the optimal location for a SNMR soundings was.

Creating noise maps are time consuming, e.g. a map as demonstrated has 38 point measurements and takes around 9 hours to measure with the current instrument. A less time consuming method, the combined point measurement method, was suggested and demonstrated with 4 point measurements, which take around 15 minutes to measure. With the combined point measurement method it is possible to locate noise sources and with that information the optimum location for a SNMR measurement is efficiently determined. Furthermore, it has been shown how the nC can help in predicting the influence of noise sources in SNMR soundings. By identifying the different noise sources in the nC data the stacksize can be determined to obtain a specified acceptable noise level.

Acknowledgements

We would like to thank Simon Ejlersen from Aarhus University for building the hardware of the nC and for very good technical support. We would also like to thank the two anonymous reviewers for their

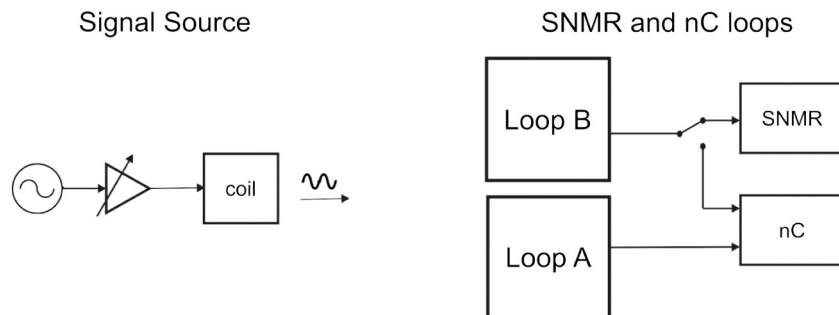


Fig. 8. Experimental setup. The signal source consists of a function generator, an amplifier and a coil. The emitted signal is detected in loop A and B. Loop A is a reference loop connected to the nC. Loop B is connected to either the SNMR system or the nC.

time spent and insightful comments helping us to improve the paper. The SNMR equipment used in this experiment is the NUMIS Poly (Iris Instruments). The use of trademarks does not imply recommendations from the authors.

This work was supported by the Danish Council for Strategic Research funded project “Nitrate Reduction in Geologically Heterogeneous Catchments” (NiCA). A project searching to identify robust agricultural areas from which only a limited part of the nitrate leached from the root zone would reach streams.

References

- Behroozmand, A.A., Auken, E., Fiandaca, G., Christiansen, A.V., Christensen, N.B., 2012. Efficient full decay inversion of MRS data with a stretched-exponential approximation of the $T2^*$ distribution. *Geophys. J. Int.* 190, 900–912.
- Bernard, J., 2007. Instruments and field work to measure a magnetic resonance sounding. *Bol. Geol. Min.* 118, 459–472.
- Dalgaard, E., Auken, E., Larsen, J.J., 2012. Adaptive noise cancelling of multichannel magnetic resonance sounding signals. *Geophys. J. Int.* 191, 88–100.
- Dlugosch, R., Müller-Petke, M., Günther, T., Costabel, S., Yaramanci, U., 2011. Assessment of the potential of a new generation of surface nuclear magnetic resonance instruments. *Near Surf. Geophys.* 9, 89–102.
- Hoaglin, D.C., Mosteller, F., Tukey, J.W., 2000. *Understanding Robust and Exploratory Data Analysis*. Wiley Classics Library, p. 447.
- Jiang, C., Lin, J., Duan, Q., Sun, S., Tian, B., 2011. Statistical stacking and adaptive notch filter to remove high-level electromagnetic noise from MRS measurements. *Near Surf. Geophys.* 9, 459–468.
- Knight, R., Grunewald, E., Irons, T., Dlubac, K., Song, Y., Bachman, H.N., Grau, B., Walsh, D., Abraham, J.D., Cannia, J., 2012. Field experiment provides ground truth for surface nuclear magnetic resonance measurement. 39.
- Larsen, J.J., Dalgaard, E., Auken, E., 2013. Noise cancelling of MRS signals combining model-based removal of powerline harmonics and multichannel Wiener filtering. *Geophys. J. Int.* 2113, 1–9 (November 7).
- Legchenko, A., Valla, P., 2003. Removal of power-line harmonics from proton magnetic resonance measurements. *J. Appl. Geophys.* 53, 103–120.
- Mukhopadhyay, S., Ray, G.C., 1998. A new interpretation of nonlinear energy operator and its efficacy in spike detection. *IEEE Trans. Biomed. Eng.* 45, 180–187.
- Müller-Petke, M., Costabel, S., 2013. Comparison and optimal parameter setting of reference-based harmonic noise cancellation in time and frequency domain for surface-NMR. *Near Surf. Geophys.* 11.
- Müller-Petke, M., Yaramanci, U., 2010. QT inversion – comprehensive use of the complete surface NMR data set. *Geophysics* 75, WA199–WA209.
- Ryom Nielsen, M., Hagensen, T.F., Chalikakis, K., Legchenko, A., 2011. Comparison of transmissivities from MRS and pumping tests in Denmark. *Near Surf. Geophys.* 9, 211–223.
- Trushkin, D.V., Shushakov, O.A., Legchenko, A.V., 1994. The potential of a noise-reducing antenna for surface NMR groundwater surveys in the Earth's magnetic field. *Geophys. Prospect.* 42, 855–862.
- Walsh, D.O., 2008. Multi-channel surface NMR instrumentation and software for 1D/2D groundwater investigations. *J. Appl. Geophys.* 66, 140–150.
- Yang, C.F., Lai, G.G., Su, C.T., Huang, H.M., 2013. Mitigation of magnetic field using three-phase four-wire twisted cables. *Int. Trans. on Electr. Energ. Syst.* 23, 13–23.